Inorganic Chemistry

pubs.acs.org/IC

Featured Article

Third-Generation W(CNAr)$_6$ Photoreductants (CNAr = Fused-Ring and Alkynyl-Bridged Arylisocyanides)

Javier Fajardo, Jr., Josef Schwan, Wesley W. Kramer, Michael K. Takase, Jay R. Winkler,* and Harry B. Gray*

Cite This: *Inorg. Chem.* 2021, 60, 3481−3491

Read Online

ACCESS | Metrics & More | Article Recommendations | Supporting Information

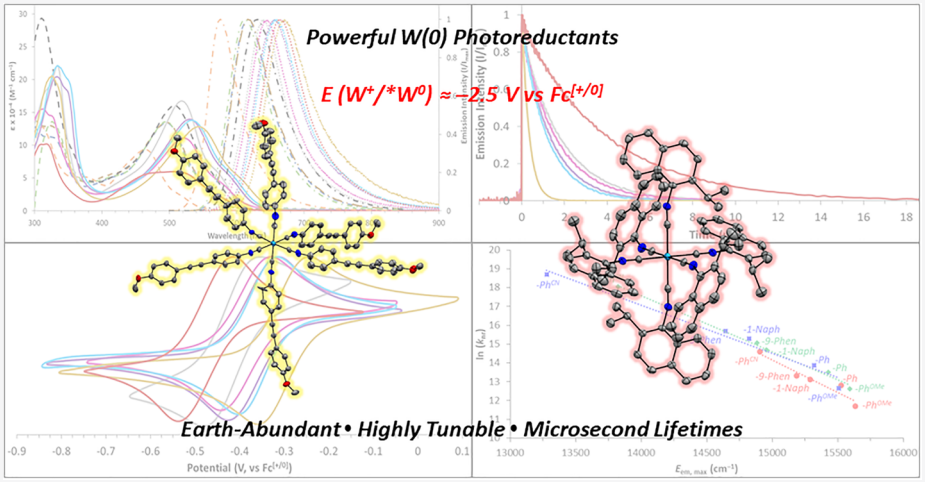

ABSTRACT: Homoleptic tungsten(0) arylisocyanides possess photophysical and photochemical properties that rival those of archetypal ruthenium(II) and iridium(III) polypyridine complexes. Previous studies established that extending the π-system of 2,6-diisopropylphenylisocyanide (CNDipp) by coupling aryl substituents *para* to the isocyanide functionality results in W(CNDippAr)$_6$ oligoarylisocyanide complexes with greatly enhanced metal-to-ligand charge transfer (MLCT) excited-state properties relative to those of W(CNDipp)$_6$. Extending electronic modifications to delineate additional design principles for this class of photosensitizers, herein we report a series of W(CNAr)$_6$ compounds with naphthalene-based fused-ring (CN-1-(2-^{i}Pr)-Naph) and CNDipp-based alkynyl-bridged (CNDipp^{CC}Ar) arylisocyanide ligands. Systematic variation of the secondary aromatic system in the CNDipp^{CC}Ar platform provides a straightforward method to modulate the photophysical properties of W(CNDipp^{CC}Ar)$_6$ complexes, allowing access to an extended range of absorption/luminescence profiles and highly reducing excited states, while maintaining the high molar absorptivity MLCT absorption bands, high photoluminescence quantum yields, and long excited-state lifetimes of previous W(CNAr)$_6$ complexes. Notably, W(CN-1-(2-^{i}Pr)-Naph)$_6$ exhibits the longest excited-state lifetime of all W(CNAr)$_6$ complexes explored thus far, highlighting the potential benefits of utilizing fused-ring arylisocyanide ligands in the construction of tungsten(0) photoreductants.

INTRODUCTION

Photoactive coordination complexes are utilized in solar energy conversion,[1] photoredox catalysis,[2,3] luminescent devices,[4] and biological imaging.[5] As a result of such breadth, the development of photosensitizers with readily tailorable photophysical and photochemical properties is of great interest. Ruthenium(II) polypyridine[6,7] and cyclometalated iridium(III) 2-phenylpyridine[8,9] complexes with low-spin 4d^6 and 5d^6 electronic configurations represent a privileged and highly modular category of molecular photosensitizers. Because these complexes can undergo visible light-induced metal-to-ligand charge transfer (MLCT) transitions that generate long-lived redox-active triplet MLCT (^{3}MLCT) states,[10] they currently dominate many photonic applications.

There is a long-standing interest in replacing precious metal-based photosensitizers with similarly tunable photoactive complexes constructed from earth-abundant elements.[11] In

Received: September 30, 2020
Published: December 6, 2020

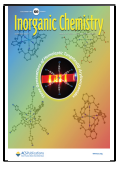

https://dx.doi.org/10.1021/acs.inorgchem.0c02912
Inorg. Chem. 2021, 60, 3481−3491

this regard, group 6 homoleptic arylisocyanide (CNAr) transition metal complexes have emerged as a novel class of low-spin d^6 photoreductants with photophysical properties that rival those of ruthenium(II) and iridium(III) coordination compounds.[12,13] For instance, remarkably photostable tris(*m*-terphenyl diisocyanide)molybdenum(0) complexes Mo(CN^{R}Ar$_3$NC)$_3$ (R = Me, ^{t}Bu) exhibit room temperature solution ^{3}MLCT lifetimes (τ) and photoluminescence quantum yields (ϕ_{PL}) of up to 1 μs and 0.2, respectively.[14] Notably, because these compounds are more powerful photoreductants ($E(Mo^+/*Mo^0) \approx -2.6$ V vs $Fc^{[+/0]}$; * denotes the lowest energy excited state; Fc = ferrocene) than *fac*-Ir(ppy)$_3$ ($E(Ir^{4+}/*Ir^{3+}) = -2.1$ V vs $Fc^{[+/0]}$), they are competent visible light photoredox catalysts for base-promoted homolytic aromatic substitution reactions as well as the rearrangement of acyl cyclopropanes to 2,3-dihydrofurans.[14,15] Similarly, Cr(CN$^{t\text{Bu}}$Ar$_3$NC)$_3$ is emissive in deaerated tetrahydrofuran (THF) solution with $\tau(^3\text{MLCT}) = 2.2$ ns, representing the first example of a $3d^6$ ^{3}MLCT room temperature photoluminescent analogue of $Fe(bpy)_3^{2+}$.[16]

Related studies by our group have established that the sterically encumbered tungsten(0) hexakis(2,6-diisopropylphenylisocyanide) complex W(CNDipp)$_6$ is also a robust, relatively long-lived ($\tau(^3\text{MLCT}) = 75$ ns in THF) excited-state reductant ($E(W^+/*W^0) = -3.0$ V vs $Fc^{[+/0]}$) capable of triggering one-electron reduction of challenging substrates, including anthracene, cobaltocenium, benzophenone, and acetophenone, upon visible light excitation.[17−20] Notably, electronic modification of CNDipp by coupling of aryl substituents *para* to the isocyanide functionality (Figure 1) leads to W(CNDippAr)$_6$ oligoarylisocyanide complexes with greatly enhanced excited-state properties. Compared to W(CNDipp)$_6$, W(CNDippPh)$_6$, W(CNDippPh^{OMe2})$_6$, W(CNDippPh^{OMe3})$_6$, and W(CNDippPh^{Ph})$_6$ feature more intense and red-shifted MLCT absorption and emission profiles, $\tau(^3\text{MLCT})$ in the microsecond range, and ϕ_{PL} up to 0.4, while retaining comparable excited-state reduction potentials.[21,22] More recently, we also found that W(CNDippAr)$_6$ complexes exhibit exceptionally high two-photon absorption cross sections (δ) in the range 1000−2000 GM (GM = Goeppert−Mayer; 1 GM = 10^{-50} cm^4 s photon^{-1} molecule^{-1}) at 812 nm,[23] making them attractive platforms for two-photon imaging[24] and near-IR two-photon redox catalysis.[25]

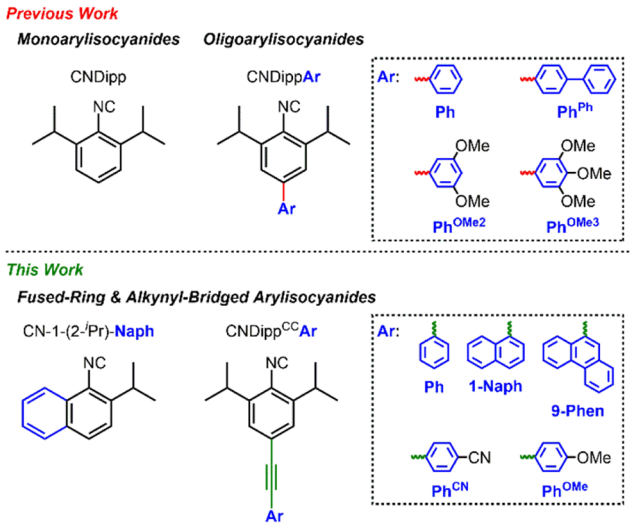

Figure 1. Arylisocyanide ligands used to prepare W(CNAr)$_6$ complexes.

Because the photophysical properties of W(CNDippAr)$_6$ complexes are strongly dependent on the identity of the appended aryl group, we became interested in further examining the effects of extension of the ligand π-system on the excited-state properties of W(CNAr)$_6$ photoreductants. In particular, red-shifting of the absorbance and luminescence bands is desirable for both photoredox and imaging purposes. Density functional theory (DFT) computations on W(CNAr)$_6$ systems (Ar = Dipp, DippPh^{OMe2}) have revealed that both the initially populated singlet MLCT (^{1}MLCT) state and the long-lived ^{3}MLCT state involve significant charge transfer from the tungsten center primarily onto the aryl component(s) of the CNAr ligands.[22] We therefore envisioned expanding the aromatic system of CNDipp through (1) the incorporation of π-bridge-containing alkynyl-aryl units at the 4-position or (2) the use of related fused-ring arylisocyanides to achieve this goal.

Herein we report a third generation of homoleptic tungsten(0) coordination compounds supported by naphthalene-based fused-ring (CN-1-(2-^{i}Pr)-Naph) and CNDipp-based alkynyl-bridged (CNDipp^{CC}Ar) arylisocyanide ligands (Figure 1). The syntheses of the latter are highly modular; through systematic variation of the secondary aromatic system, we demonstrate that simple substitutions on the CNDipp^{CC}Ar platform provide a straightforward method to tune the ground- and excited-state properties of W(CNDipp^{CC}Ar)$_6$ complexes. Importantly, these complexes display an extended range of absorption/luminescence profiles and highly reducing excited states, while maintaining the high molar absorptivity MLCT absorption bands, high photoluminescence quantum yields, and long excited-state lifetimes of previous W(CNAr)$_6$ complexes. Notably, W(CN-1-(2-^{i}Pr)-Naph)$_6$ exhibits the longest excited-state lifetime of all W(CNAr)$_6$ complexes explored thus far, highlighting the potential benefits of utilizing fused-ring arylisocyanide ligands in the design of tungsten(0) photoreductants.

EXPERIMENTAL SECTION

General Considerations. All manipulations were carried out using standard Schlenk or glovebox techniques under an inert atmosphere (dinitrogen or argon). Solvents were deoxygenated and dried by thoroughly sparging with N_2 gas, followed by passage through an activated alumina column in the solvent purification system by SG Water USA, LLC. Nonhalogenated solvents were tested with sodium benzophenone ketyl in THF in order to confirm effective oxygen and moisture removal. Deuterated solvents were purchased from Cambridge Isotope Laboratories, Inc., degassed, and dried over activated 3 Å molecular sieves prior to use.

For chemical precursors and detailed synthetic procedures, see the Supporting Information.

Spectroscopic Methods. Nuclear magnetic resonance (NMR) measurements were performed at room temperature on a Varian 300 or 400 MHz spectrometer. ^{1}H and ^{13}C{^{1}H} NMR chemical shifts are reported in parts per million (ppm) relative to tetramethylsilane, using residual ^{1}H and ^{13}C resonances from the solvent as internal standards.

Infrared (IR) spectra of free CNAr ligands and their formamide precursors were obtained on thin films, formed by the evaporation of solutions on KBr plates, using a PerkinElmer Spectrum BXII spectrometer. IR spectra of free CNAr ligands and W(CNAr)$_6$ complexes were obtained on thin films, formed by the evaporation

https://dx.doi.org/10.1021/acs.inorgchem.0c02912
Inorg. Chem. 2021, 60, 3481−3491

of solutions, using a Bruker Alpha Platinum ATR spectrometer with *OPUS* software in a glovebox under an N_2 atmosphere.

UV−visible absorption measurements were performed under an N_2 atmosphere at room temperature using a Cary 50 UV−visible spectrophotometer. Samples were prepared in dry, degassed solvents inside a nitrogen-filled glovebox, placed in the cell of a high-vacuum 1 cm path-length fused quartz cuvette (Starna Cells), and isolated from atmosphere by a high-vacuum Teflon valve (Kontes). All samples had a blank sample background subtraction applied.

Steady-state and time-resolved luminescence measurements were performed under an N_2 atmosphere. The measurements were carried out in the Beckman Institute Laser Resource Center at Caltech. Steady-state emission spectra were recorded on a modified Jobin Yvon Spec Fluorolog-3-11. Sample excitation was achieved via a xenon arc lamp with wavelength selection provided by a monochromator. Luminescence was collected at 90° to the excitation direction and directed by a bifurcated optical fiber bundle to two Ocean Optics QEPro CCD spectrometers spanning 300−930 nm. Spectra were corrected for instrument response. Photoluminescence quantum yield measurements were performed as described previously.[21] Steady-state emission measurements at 77 K were performed by immersing quartz electron paramagnetic resonance (EPR) tubes containing glassed samples of $W(CNAr)_6$ complexes (toluene or 2-methyltetrahydrofuran (2-MeTHF)) in a glass dewar filled with liquid nitrogen.

The 77 K luminescence spectra were fit to a Franck−Condon spectroscopic model using one classical distorting mode and two or three quantum mechanical distorting modes.[26,27] The vibrational frequencies of the distorting modes were assumed to be identical in the ground and excited electronic states. The classical mode distortion was represented by a Gaussian function with full-width at half-maximum (fwhm; cm^{-1}) $\approx 503\lambda_{classical}$ (cm^{-1}). The energy maximum of the Gaussian for the transition from the quantum mechanical vibrationally unexcited ground electronic state to the quantum mechanical vibrationally unexcited luminescent electronic state is defined as the parameter E_{00}. Distortions in the quantum mechanical vibrational mode i (i = 1−3) of frequency ω_i are described by the Huang−Rhys parameter S_i. Fits were optimized by least-squares minimization using the parameters E_{00}, $\lambda_{classical}$, ω_i, and S_i.

For time-resolved measurements, laser excitation was provided by 8 ns pulses from a Q-switched Nd:YAG laser (Spectra-Physics Quanta-Ray PRO-Series) operating at 10 Hz. The second harmonic was used to provide laser pulses at 532 nm. After passing through the sample collinearly with the laser beam, scattered excitation light was rejected by suitable long-pass and short-pass filters, and probe wavelengths were selected for detection by a double monochromator (Instruments SA DH-10) with 1 mm slits. Data were averaged over approximately 100 shots. All instruments and electronics in these systems were controlled by software written in *LabVIEW* (National Instruments). Time-resolved luminescence measurements at 77 K were performed by immersing quartz EPR tubes containing glassed samples of $W(CNAr)_6$ complexes (toluene or 2-MeTHF) in a glass dewar filled with liquid nitrogen.

Electrochemistry. Electrochemical measurements were performed at room temperature and carried out in a glovebox under an N_2 atmosphere in a one-compartment cell using a Biologic SP-200 potentiostat. A platinum wire was used as the working electrode and a carbon rod was used as the auxiliary electrode. A silver pseudoreference electrode was used with the ferrocene couple ($Fc^{[+/0]}$) as an internal reference. THF solutions of electrolyte (0.1 M [^{n}Bu$_4$][PF_6]) and analyte (ca. 1 mM) were also prepared under an N_2 atmosphere.

X-ray Crystallography. X-ray diffraction (XRD) studies were carried out at the Caltech Beckman Institute X-ray Crystallography Facility on a Bruker AXS KAPPA APEXII (Mo Kα radiation) or a Bruker AXS D8 VENTURE (Mo Kα or Cu Kα) diffractometer. Structures were solved by direct methods using *SHELXS*[28] and refined against F^2 on all data by full-matrix least-squares with *SHELXL-2017*[29] using established refinement techniques.[30] All non-hydrogen atoms were refined anisotropically. All hydrogen atoms were included in the model at geometrically calculated positions and refined using a riding model. The isotropic displacement parameters of all hydrogen atoms were fixed to 1.2 times the U value of the atoms they are linked to (1.5 times for methyl groups). All disordered atoms were refined with the help of similarity restraints on the 1,2- and 1,3-distances and displacement parameters, as well as enhanced rigid bond restraints for anisotropic displacement parameters.

For additional refinement details, see the Supporting Information.

RESULTS AND DISCUSSION

Synthesis and Characterization of $W(CNDipp^{CC}Ar)_6$ and $W(CN\text{-}1\text{-}(2\text{-}^i Pr)\text{-}Naph)_6$ Complexes. The $CNDipp^{CC}Ar$ and CN-1-(2-^{i}Pr)-Naph arylisocyanide ligands of interest in this work are depicted in Figure 1. The former were prepared according to modified literature procedures.[21,31,32] Like their CNDippAr counterparts, all $CNDipp^{CC}Ar$ ligands can be prepared from the same readily accessible synthetic intermediate, *N*-formyl-4-iodo-2,6-diisopropylaniline. Sonogashira coupling of this reagent with phenylacetylene, 1-naphthylacetylene, 9-phenanthrenylacetylene, 4-methoxyphenylacetylene, or 4-cyanophenylacetylene, followed by dehydration of the resulting formamide with $OPCl_3$, yields the isocyanide ligands $CNDipp^{CC}Ph$, $CNDipp^{CC}$-1-Naph, $CNDipp^{CC}$-9-Phen, $CNDipp^{CC}Ph^{OMe}$, and $CNDipp^{CC}Ph^{CN}$, respectively, in moderate yield (Scheme 1). These ligands display strong, sharp IR

Scheme 1. Synthesis of $CNDipp^{CC}Ar$ and CN-1-(2-^{i}Pr)-Naph Ligands

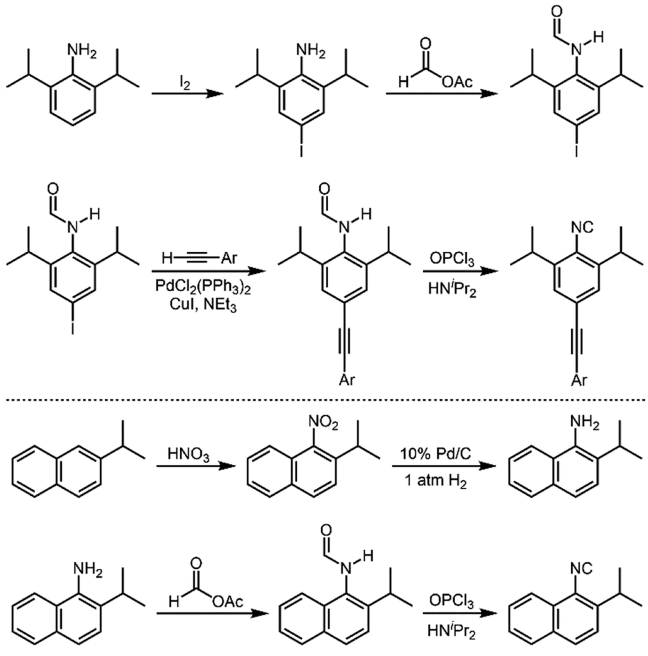

ν(CN) isocyanide absorption bands in the narrow range 2109−2114 cm^{-1}, as well as similar isocyanide (173.3−174.0 ppm) and alkyne (88.5−94.4 ppm) ^{13}C NMR chemical shifts. The ν(CC) alkyne stretching frequencies also span a small range (2204−2213 cm^{-1}) but vary from weak ($CNDipp^{CC}Ph$, $CNDipp^{CC}$-1-Naph, and $CNDipp^{CC}$-9-Phen) to medium ($CNDipp^{CC}Ph^{OMe}$ and $CNDipp^{CC}Ph^{CN}$) intensity. A strong nitrile ν(CN) vibration is observed in the IR spectrum of $CNDipp^{CC}Ph^{CN}$ at 2228 cm^{-1}.

Fused-ring 2-isopropyl-1-naphthylisocyanide was prepared according to the multistep synthesis in Scheme 1. Nitration of 2-isopropylnaphthalene occurs unselectively, requiring separa-

https://dx.doi.org/10.1021/acs.inorgchem.0c02912
Inorg. Chem. 2021, 60, 3481−3491

tion of the desired 2-isopropyl-1-nitronaphthalene isomer by column chromatography. Subsequent Pd/C-catalyzed reduction of the nitro group with H_2(g) affords the key intermediate (2-isopropyl-1-naphthyl)amine.[33,34] Formylation, followed by dehydration, then yields CN-1-(2-^{i}Pr)-Naph, which exhibits a sharp ν(CN) stretching frequency at 2114 cm^{-1} with a shoulder at 2092 cm^{-1} and a diagnostic ^{13}C NMR chemical shift at 172.7 ppm for the isocyanide carbon.

Reductive metalation of CNDipp^{CC}Ar ligands (Ar = Ph, 1-Naph, 9-Phen) with $WCl_4(THF)_2$ and sodium amalgam (Na(Hg)) in the dark proceeds smoothly in room temperature THF solution over the course of several hours to yield magenta W(CNDipp^{CC}Ar)$_6$ (Scheme 2). The use of CNDipp^{CC}Ph^{OMe} affords W(CNDipp^{CC}Ph^{OMe})$_6$ as red needles after crystallization from pentane/benzene solution. Interestingly, W(CNDipp^{CC}Ph^{CN})$_6$ does not form under these conditions. Instead, reduction of a mixture of CNDipp^{CC}Ph^{CN} and $WCl_4(THF)_2$ in THF with Zn^0 affords W(CNDipp^{CC}Ph^{CN})$_6$ as a dark-violet solid after purification (Scheme 2).

Scheme 2. Synthesis of W(CNDipp^{CC}Ar)$_6$ and W(CN-1-(2-^{i}Pr)-Naph)$_6$ Complexes[a]

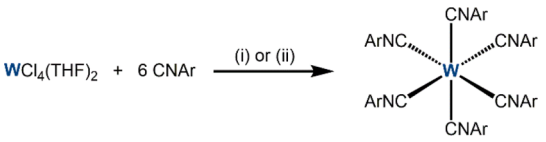

[a](i) CNAr = CNDipp^{CC}Ar (Ar = Ph, 1-Naph, 9-Phen, Ph^{OMe}) or CN-1-(2-^{i}Pr)-Naph: Na(Hg), THF; (ii) CNAr = CNDipp^{CC}Ph^{CN}: Zn^0, THF.

Initial attempts to prepare homoleptic tungsten(0) fused-ring arylisocyanide complexes under similar reaction conditions using 2-naphthylisocyanide (CN-2-Naph) or 1-naphthylisocyanide (CN-1-Naph) were largely unsuccessful. While the formation of W(CN-2-Naph)$_6$ and W(CN-1-Naph)$_6$ was confirmed by ^{1}H NMR and IR spectroscopy and single-crystal XRD (see the Supporting Information), they could not be isolated in quantity. In contrast, the reduction of $WCl_4(THF)_2$ by Na(Hg) in the presence of more sterically hindered CN-1-(2-^{i}Pr)-Naph yielded W(CN-1-(2-^{i}Pr)-Naph)$_6$ as dark-red needles in high isolated yield following crystallization from a room temperature pentane/C_6H_6 solution (Scheme 2). The greater stability of W(CN-1-(2-^{i}Pr)-Naph)$_6$ versus W(CN-2-Naph)$_6$ and W(CN-1-Naph)$_6$ is consistent with the presence of sterically demanding substituents at both positions *ortho* to the isocyanide, which preclude potential tungsten-mediated CNAr coupling decomposition pathways,[35] and is in line with previous findings from our group that incorporation of increasingly bulky groups at the 2- and 6-positions of monoarylisocyanides results in greater stability of W(CNAr)$_6$ complexes (Ar = Dipp > Xy > Ph; Xy = 2,6-dimethylphenyl).[18−20]

W(CN-1-(2-^{i}Pr)-Naph)$_6$ and all W(CNDipp^{CC}Ar)$_6$ complexes display a single set of ^{1}H and ^{13}C NMR resonances for the isocyanide ligands in C_6D_6, indicating high symmetry in solution. While the isocyanide (CN-1-(2-^{i}Pr)-Naph: 179.6 ppm; CNDipp^{CC}Ar: 177.0−177.1 ppm) and alkyne (89.0−95.8 ppm) ^{13}C NMR resonances of the complexes do not shift

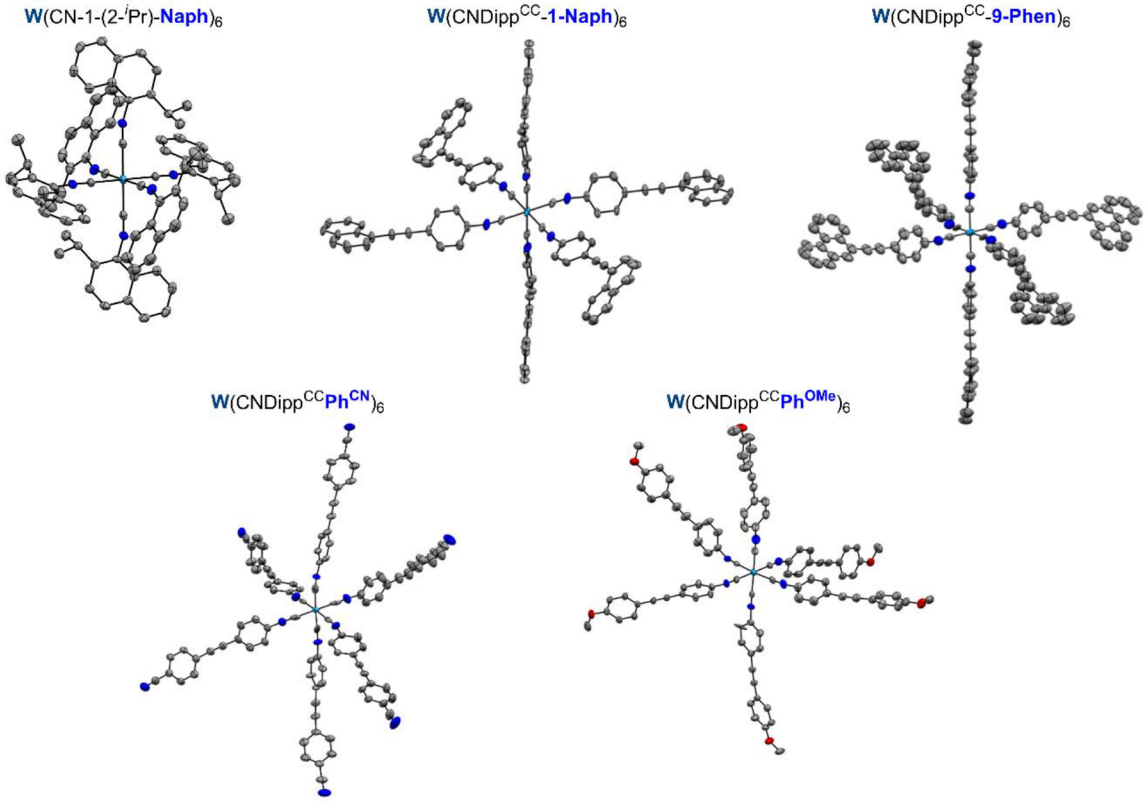

Figure 2. Solid-state structures of W(CN-1-(2-^{i}Pr)-Naph)$_6$ and W(CNDipp^{CC}Ar)$_6$ complexes with thermal ellipsoids set at 50% probability. The isopropyl groups of the W(CNDipp^{CC}Ar)$_6$ complexes, cocrystallized solvents, hydrogen atoms, and the minor component of the disorder are omitted for clarity. Atom color code: W, teal; N, blue; O, red; C, gray.

https://dx.doi.org/10.1021/acs.inorgchem.0c02912
Inorg. Chem. 2021, 60, 3481−3491

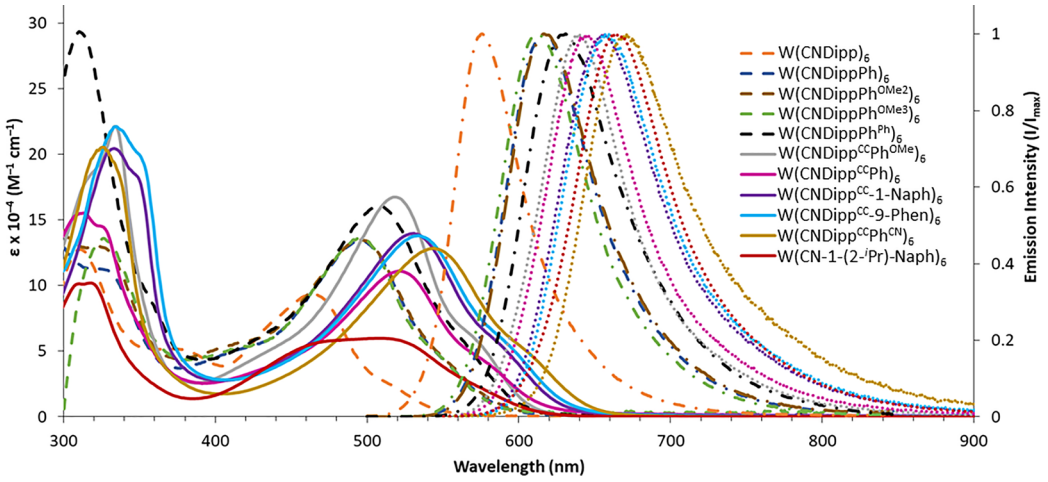

Figure 3. Absorption and emission spectra of W(CNDipp^{CC}Ar)$_6$ and W(CN-1-(2-^{i}Pr)-Naph)$_6$ complexes in deaerated room temperature toluene solution. Spectra of W(CNDipp)$_6$ and W(CNDippAr)$_6$ (from ref 21) plotted for comparison.

significantly from values for the corresponding free ligands, the complexes display diagnostic broad, intense ν(CN) at lower frequencies (1934−1944 cm^{-1}), consistent with enhanced π-back-donation from tungsten(0) upon coordination of the arylisocyanides.

Single-crystal XRD studies confirmed the identities of W(CNDipp^{CC}Ar)$_6$ complexes (Ar = 1-Naph, 9-Phen, Ph^{OMe}, Ph^{CN}); their structures are illustrated in Figure 2. The structures invariably suffer from poor resolution and/or disorder, and only the major component of the disorder is shown. Attempts to obtain higher-quality structures by growing crystals under different sets of conditions were unsuccessful. Thus, the disorder and poor resolution of the W(CNDipp^{CC}Ar)$_6$ structures preclude a detailed discussion of their molecular metrics. Single crystals suitable for XRD analysis could not be obtained for W(CNDipp^{CC}Ph)$_6$.

In contrast, W(CN-1-(2-^{i}Pr)-Naph)$_6$ crystallizes in the space group $P\bar{1}$ without any disorder (Figure 2). This complex displays W−C (2.068(3), 2.070(3), and 2.084(3) Å) and C≡N (1.171(4), 1.170(4), and 1.164(4) Å) bond lengths, as well as C$_{isocyanide}$−N−C$_{aryl}$ bond angles (159.7(3)°, 159.6(3)°, and 166.7(3)°), comparable to those of W(CNDipp)$_6$ and W(CNDippAr)$_6$ compounds (Ar = Ph, Ph^{OMe2}, Ph^{OMe3}, Ph^{Ph}).[20,21] The geometry around the tungsten center is close to octahedral, with C−W−C angles of 88.29(11)°, 89.69(11)°, and 92.34(12)°. W(CNDipp^{CC}-1-Naph)$_6$ and W(CNDipp^{CC}Ph^{OMe})$_6$, which only feature minor disorder in their W(C≡N−C$_{aryl}$)$_6$ core, also display similar bond lengths and angles. Further inspection of the solid-state structure of W(CN-1-(2-^{i}Pr)-Naph)$_6$ reveals that, in addition to effectively shielding the metal center, the sterics afforded by the naphthyl and isopropyl groups flanking the isocyanide functionality constrain the ligands, and thus likely impart considerable rigidity to the complex relative to W(CNDipp)$_6$, W(CNDippAr)$_6$, and W(CNDipp^{CC}Ar)$_6$.

We have previously established that the conformation of the *trans* arylisocyanide aromatic systems determines the degree of conjugation along a given molecular axis and, consequently, the location of the lowest energy MLCT absorption maximum.[22] Importantly, the use of bulky *ortho* isopropyl groups in W(CNDipp)$_6$ and W(CNDippAr)$_6$ (Ar = Ph, Ph^{OMe2}, Ph^{OMe3}, Ph^{Ph}) has been observed to enforce approximately coplanar *trans* CNDipp π-systems, resulting in the fully conjugated orientation being the lowest energy conformation.[20,21] W(CN-1-(2-^{i}Pr)-Naph)$_6$, W(CNDipp^{CC}-1-Naph)$_6$, W(CNDipp^{CC}-9-Phen)$_6$, and W(CNDipp^{CC}Ph^{CN})$_6$ follow this trend, displaying nearly coplanar *trans* naphthyl- and 2,6-diisopropylphenylisocyanide aromatic systems, respectively (Figure 2). Interestingly, the CNDipp π-systems of W(CNDipp^{CC}Ph^{OMe})$_6$ are instead closer to orthogonal, despite the presence of isopropyl substituents at both *ortho* positions. However, the electronic absorption spectrum of this complex (Figure 3) closely resembles that of W(CNDippAr)$_6$ and W(CNDipp^{CC}Ar)$_6$ congeners rather than that of W(CNXy)$_6$, where the *trans* CNXy ligands are roughly orthogonal.[36] We tentatively ascribe this discrepancy to crystal packing effects, as one molecule of C_6H_6 cocrystallizes in the vicinity of two CNDipp fragments of W(CNDipp^{CC}Ph^{OMe})$_6$ and likely influences the observed orientations (Figure S207). It is also worth noting that for W(CNXy)$_6$, W(CNDipp)$_6$, and W(CNDippAr)$_6$, both orthogonal and coplanar conformers are present in solution, albeit with appreciably different populations.[22]

In addition to the CNDipp π-systems proximal to the tungsten center, the orientation of the peripheral aromatic systems in the alkynyl-bridged W(CNDipp^{CC}Ar)$_6$ complexes also influences the degree of conjugation along the molecular axes, which, in turn, affects the spectroscopic and photophysical properties. With relation to the coordinated CNDipp fragment for a given individual ligand, the 1-Naph, 9-Phen, Ph^{OMe}, and Ph^{CN} secondary π-systems adopt a distribution of conformations ranging from nearly coplanar to approximately orthogonal, as determined by the dihedral angle between the mean planes defined by the corresponding aryl rings ($\varphi_{Ar1-Ar2}$; Ar1 = Dipp). The average $\varphi_{Ar1-Ar2}$ values in the series of W(CNDipp^{CC}Ar)$_6$ compounds are 37.7° (Ar2 = 1-Naph), 34.6° (Ar2 = 9-Phen), 31.5° (Ar2 = Ph^{OMe}), and 56.1° (Ar2 = Ph^{CN}).[37] The distribution of conformers observed for these compounds in the solid state is in line with the low rotational barrier for unhindered diarylacetylene-type moieties.[38] For comparison, the average dihedral angles for W(CNDippPh)$_6$, W(CNDippPh^{Ph})$_6$, and W(CNDippPh^{OMe2})$_6$ are ca. 35°, and that of W(CNDippPh^{OMe3})$_6$ is 51°.[21]

Absorption and Steady-State Luminescence Spectra. W(CNAr)$_6$ compounds (Ar = Ph, Xy, Dipp) display high molar absorptivity MLCT absorption bands in the visible

https://dx.doi.org/10.1021/acs.inorgchem.0c02912
Inorg. Chem. 2021, 60, 3481−3491

Table 1. Absorption and Emission Properties of $W(CNAr)_6$ Complexes[a]

$W(CNAr)_6$	toluene			2-MeTHF		THF	
	$\varepsilon_{\lambda,max}$[c] {$\lambda_{abs,max}$}[d]	$\lambda_{em,max}$[d] {$E_{em,max}$}[e]	fwhm[e]	$\lambda_{em,max}$[d] {$E_{em,max}$}[e]	fwhm[e]	$\lambda_{em,max}$[d] {$E_{em,max}$}[e]	fwhm[e]
$W(CNDipp)_6$[b]	9.5×10^4 {465}	575 {17300}	1610			577 {17300}	1750
$W(CNDippPh)_6$[b]	1.3×10^5 {495}	617 {16200}	1880			626 {15900}	2250
$W(CNDippPh^{OMe2})_6$[b]	1.3×10^5 {495}	618 {16100}	1890			627 {15800}	2280
$W(CNDippPh^{OMe3})_6$[b]	1.3×10^5 {495}	612 {16300}	1850			623 {16000}	2180
$W(CNDippPh^{Ph})_6$[b]	1.6×10^5 {506}	629 {15800}	1970			656 {15200}	2670
$W(CNDipp^{CC}Ph^{OMe})_6$	1.6×10^5 {518}	640 {15600}	1610	642 {15600}	1780	645 {15500}	1850
$W(CNDipp^{CC}Ph)_6$	1.1×10^5 {521}	644 {15500}	1670	648 {15400}	1880	653 {15300}	1980
$W(CNDipp^{CC}$-1-Naph$)_6$	1.4×10^5 {531}	653 {15300}	1780	669 {15000}	2120	675 {14800}	2300
$W(CNDipp^{CC}$-9-Phen$)_6$	1.4×10^5 {533}	658 {15200}	1780	672 {14900}	2150	683 {14600}	2350
$W(CNDipp^{CC}Ph^{CN})_6$	1.3×10^5 {544}	671 {14900}	1770	723 {13800}	2990	753 {13300}	3510
W(CN-1-(2-^{i}Pr)-Naph$)_6$	5.7×10^4 {509}	664 {15100}	1680	670 {14900}	1910	671 {14900}	1990

[a]Collected from deaerated room temperature solutions. [b]Data from ref 21. [c]In M^{-1} cm^{-1}. [d]In nm. [e]In cm^{-1}.

Table 2. Excited-State Decay Parameters of $W(CNAr)_6$ Complexes[a]

$W(CNAr)_6$	toluene				THF			
	τ[c]	ϕ_{PL}	k_r[d]	k_{nr}[d]	τ[c]	ϕ_{PL}	k_r[d]	k_{nr}[d]
$W(CNDipp)_6$[b]	0.12	0.03	2.3×10^5	8.0×10^6	0.08	0.01	1.6×10^5	1.3×10^7
$W(CNDippPh)_6$[b]	1.73	0.41	2.4×10^5	3.4×10^5	1.32	0.21	1.6×10^5	6.0×10^5
$W(CNDippPh^{OMe2})_6$[b]	1.65	0.42	2.6×10^5	3.5×10^5	1.20	0.21	1.8×10^5	6.6×10^5
$W(CNDippPh^{OMe3})_6$[b]	1.83	0.41	2.2×10^5	3.2×10^5	1.56	0.25	1.6×10^5	4.8×10^5
$W(CNDippPh^{Ph})_6$[b]	1.53	0.44	2.9×10^5	3.7×10^5	0.35	0.07	1.9×10^5	2.7×10^6
$W(CNDipp^{CC}Ph^{OMe})_6$	1.82	0.78	4.3×10^5	1.2×10^5	1.45	0.55	3.8×10^5	3.1×10^5
$W(CNDipp^{CC}Ph)_6$	1.75	0.37	2.1×10^5	3.6×10^5	0.80	0.16	2.0×10^5	1.0×10^6
$W(CNDipp^{CC}$-1-Naph$)_6$	1.45	0.30	2.0×10^5	4.8×10^5	0.22	0.05	2.1×10^5	4.3×10^6
$W(CNDipp^{CC}$-9-Phen$)_6$	1.24	0.26	2.1×10^5	6.0×10^5	0.15	0.03	2.2×10^5	6.4×10^6
$W(CNDipp^{CC}Ph^{CN})_6$	0.36	0.23	6.3×10^5	2.2×10^6	0.008	<0.01	7.5×10^5	1.3×10^8
W(CN-1-(2-^{i}Pr)-Naph$)_6$	3.83	0.25	6.5×10^4	2.0×10^5	2.15	0.11	5.3×10^4	4.1×10^5

[a]Collected from deaerated room temperature solutions. For excited-state decay parameters in 2-MeTHF, see Table S3. [b]Data from ref 21. [c]In μs. [d]In s^{-1}.

region.[17−20,22] Gratifyingly, we previously found that employment of CNDippAr ligands in place of CNDipp leads to both bathochromic shifts and increases in the intensities of the lowest energy MLCT absorption maxima for $W(CNDippAr)_6$ complexes.[21] For example, the MLCT transition shifts from $\lambda_{abs,max}$ = 465 nm with $\varepsilon_{465} = 9.5 \times 10^4$ M^{-1} cm^{-1} for the base complex $W(CNDipp)_6$ to $\lambda_{abs,max}$ = 495 nm with $\varepsilon_{495} = 1.3 \times 10^5$ M^{-1} cm^{-1} for the biarylisocyanide complexes $W(CNDippPh)_6$, $W(CNDippPh^{OMe2})_6$, and $W(CNDippPh^{OMe3})_6$ (Figure 3 and Table 1). Further red-shifting ($\lambda_{abs,max}$ = 506 nm) and increased MLCT band intensity ($\varepsilon_{506} = 1.6 \times 10^5$ M^{-1} cm^{-1}) are observed for $W(CNDippPh^{Ph})_6$.

Given these observations, we reasoned that replacing the biaryl $C(sp^2)-C(sp^2)$ linkage in CNDippAr, which limits the degree of coplanarity that can be achieved, with an alkyne π-bridge would lead to increased conjugation and more favorable optical properties. Consistent with its deep-magenta color in solution, the lowest energy MLCT absorption maximum for $W(CNDipp^{CC}Ph)_6$ occurs at $\lambda_{abs,max}$ = 521 nm in toluene, which is bathochromically shifted by 26 nm from that of its biphenylisocyanide analogue $W(CNDippPh)_6$ (Figure 3 and Table 1). Satisfyingly, this maximum also occurs at lower energy than that of $W(CNDippPh^{Ph})_6$, the most conjugated oligoarylisocyanide complex studied previously.

Increasing the peripheral aromatic system of $W(CNDipp^{CC}Ar)_6$ from Ar = Ph to Ar = 1-Naph or 9-Phen leads to further red-shifts in the MLCT band maxima; these occur at $\lambda_{abs,max}$ = 531 and 533 nm for $W(CNDipp^{CC}$-1-Naph$)_6$ and $W(CNDipp^{CC}$-9-Phen$)_6$, respectively. The addition of a nitrile group at the 4-position of the phenyl group (Ar = Ph^{CN}) results in an even greater shift to lower energy, with $W(CNDipp^{CC}Ph^{CN})_6$ displaying an MLCT maximum at $\lambda_{abs,max}$ = 544 nm. In contrast, $W(CNDipp^{CC}Ph^{OMe})_6$, incorporating an electron-donating methoxy group, leads to a slight blue-shift relative to $W(CNDipp^{CC}Ph)_6$ (Figure 3 and Table 1). These band positions correlate with the increasing electron-withdrawing nature of the secondary aromatic system in the order Ph^{OMe} < Ph < 1-Naph ≈ 9-Phen < Ph^{CN}, as gauged by their Hammett constants (taking Ar = Ph as the base complex),[39] and are consistent with the MLCT nature of the transition. Importantly, these $W(CNDipp^{CC}Ar)_6$ complexes maintain similarly high extinction coefficients (ε = (1.1−1.6) × 10^5 M^{-1} cm^{-1}) as their oligoarylisocyanide relatives (Table 1). It is also worth noting that the absorption traces of all $W(CNDipp^{CC}Ar)_6$ complexes resemble those of the $W(CNDippAr)_6$ variants, suggesting that in solution the *trans* CNDipp π-systems of $W(CNDipp^{CC}Ph^{OMe})_6$ predominantly adopt a coplanar conformation, unlike the structure in the solid state.

The fused-ring arylisocyanide CN-1-(2-^{i}Pr)-Naph provides an orthogonal approach for increasing conjugation, whereby rather than attachment of a second phenyl group to CNDipp via a $C(sp^2)-C(sp^2)$ or C(sp)−C(sp) linkage, it is fused to the primary aryl fragment. In toluene solution, W(CN-1-(2-^{i}Pr)-Naph$)_6$ absorbs in the region 460−520 nm, with a maximum at

https://dx.doi.org/10.1021/acs.inorgchem.0c02912
Inorg. Chem. 2021, 60, 3481−3491

509 nm (Figure 3). Interestingly, the extinction coefficient at this wavelength (ε_{509} = 5.7 × 10^4 M^{-1} cm^{-1}) is roughly half that of W(CNDippAr)$_6$ and W(CNDipp^{CC}Ar)$_6$ complexes at their corresponding maxima (Table 1), possibly a consequence of the loss of 3-fold degeneracy of the excited states.

As for W(CNDippAr)$_6$ complexes, the absorption profiles of W(CN-1-(2-^{i}Pr)-Naph)$_6$ and W(CNDipp^{CC}Ar)$_6$ compounds are mostly unchanged in the more polar solvents 2-MeTHF and THF. The extinction coefficients measured in the latter are similar to those in toluene (Figure S135), consistent with the near-octahedral symmetry of the complexes.

Normalized luminescence spectra of W(CNDipp^{CC}Ar)$_6$ and W(CN-1-(2-^{i}Pr)-Naph)$_6$ complexes acquired from dilute, deaerated toluene solutions under an inert N_2 atmosphere are shown in Figure 3. For comparison, emission spectra of parent W(CNDipp)$_6$ and oligoarylisocyanides W(CNDippAr)$_6$ are also plotted. The luminescence traces of all W(CNDipp)$_6$-type complexes are similar in shape. In toluene solution, the emission profiles of W(CNDipp^{CC}Ar)$_6$ compounds mirror the trend observed in their absorption spectra. For instance, the emission maximum of W(CNDipp^{CC}Ph)$_6$ ($\lambda_{em,max}$ = 644 nm) is red-shifted from that of W(CNDippPh)$_6$ ($\lambda_{em,max}$ = 617 nm). Similarly, within the W(CNDipp^{CC}Ar)$_6$ series, the emission maxima move to longer wavelengths in the order Ph^{OMe} (640 nm) < Ph (644 nm) < 1-Naph (653 nm) < 9-Phen (658 nm) < Ph^{CN} (671 nm; Figure 3 and Table 1). Structurally unique W(CN-1-(2-^{i}Pr)-Naph)$_6$ does not follow this pattern and instead luminesces with $\lambda_{em,max}$ = 664 nm. Notably, with the inclusion of these new tungsten(0) arylisocyanides, the toluene absorption and emission profiles can readily be tuned by ca. 80 and 100 nm, respectively, through the appropriate choice of an arylisocyanide ligand.

W(CNDipp^{CC}Ar)$_6$ compounds in toluene solution are highly emissive (Table 2). W(CNDipp^{CC}Ph)$_6$ exhibits ϕ_{PL} = 0.37, comparable to ϕ_{PL} = 0.41 for its biarylisocyanide analogue W(CNDippPh)$_6$. Interestingly, increasing the π-accepting ability of the secondary aryl system in W(CNDipp^{CC}Ar)$_6$ results in systematic decrease of ϕ_{PL}, with Ar = 1-Naph, 9-Phen, and Ph^{CN} variants displaying photoluminescence quantum yields of 0.30, 0.26, and 0.23, respectively. These values are lower and cover a larger range than those of W(CNDippAr)$_6$ complexes (0.41−0.44) in the same solvent. Surprisingly, the addition of a methoxy substituent to CNDipp^{CC}Ph has an even more substantial effect, doubling the measured quantum yield to ϕ_{PL} = 0.78 for W(CNDipp^{CC}Ph^{OMe})$_6$. The reason for this enhancement is not readily apparent. With the inclusion of W(CN-1-(2-^{i}Pr)-Naph)$_6$ (ϕ_{PL} = 0.25), these quantum yields are all substantially greater than that of parent W(CNDipp)$_6$ (ϕ_{PL} = 0.03) or Ru(bpy)$_3^{2+}$ (ϕ_{PL} = 0.062 in MeCN) and comparable to that of *fac*-Ir(ppy)$_3$ (ϕ_{PL} = 0.38 in MeCN).

In contrast to their absorption properties, the luminescence profiles of W(CNDipp^{CC}Ar)$_6$ and W(CN-1-(2-^{i}Pr)-Naph)$_6$ complexes are highly dependent on the polarity of the solvent. In general, their behavior in 2-MeTHF and THF parallels that of their W(CNDippAr)$_6$ relatives. For example, upon moving to 2-MeTHF, the emission bands of W(CNDipp^{CC}Ar)$_6$ and W(CN-1-(2-^{i}Pr)-Naph)$_6$ compounds red-shift and broaden (Table 1 and Figure S153). These changes are more prominent in THF, which has a higher dielectric constant (Table 1 and Figure S154), and support the assignment of an MLCT excited state. A comparison of $E_{em,max}$ and the fwhm of luminescence traces in toluene versus THF solution suggests that W(CN-1-(2-^{i}Pr)-Naph)$_6$ ($\Delta E_{em,max}$ = 150 cm^{-1}; Δfwhm = 300 cm^{-1}) and W(CNDipp^{CC}Ph)$_6$ ($\Delta E_{em,max}$ = 210 cm^{-1}; Δfwhm = 310 cm^{-1}) behave much like the biarylisocyanide complexes W(CNDippAr)$_6$ (Ar = Ph, Ph^{OMe2}, Ph^{OMe3}; $\Delta E_{em,max}$ = 230−290 cm^{-1}; Δfwhm = 330−390 cm^{-1}). In turn, the changes are greater for W(CNDipp^{CC}-1-Naph)$_6$ and W(CNDipp^{CC}-9-Phen)$_6$, with $\Delta E_{em,max}$ = 470 and 540 cm^{-1} and Δfwhm = 530 and 570 cm^{-1}, respectively. These values imply that the more extended aromatic systems exhibit larger excited-state dipoles, consistent with the DFT predictions for the lowest triplet excited states of W(CNDipp)$_6$ and W(CNDippPh^{OMe2})$_6$.[22]

W(CNDipp^{CC}Ph^{CN})$_6$ exhibits the most drastic alterations in $E_{em,max}$ and fwhm upon moving from toluene to THF; the emission maximum red-shifts by 1630 cm^{-1}, and the fwhm increases by 1740 cm^{-1} (Table 1). These changes are substantially greater than those for W(CNDipp^{CC}-1-Naph)$_6$, W(CNDipp^{CC}-9-Phen)$_6$, and W(CNDippPh^{Ph})$_6$ ($\Delta E_{em,max}$ = 650 cm^{-1}; Δfwhm = 700 cm^{-1}). We attribute these shifts to the greater electron-withdrawing capacity of the Ph^{CN} group and its ability to interact with solvent via the nitrile functionality. Interestingly, luminescence from W(CNDipp^{CC}Ph^{OMe})$_6$ is only minimally perturbed by the polarity of the solvent ($\Delta E_{em,max}$ = 130 cm^{-1}; Δfwhm = 240 cm^{-1}; Table 1).

The photoluminescence quantum yields of W(CNDipp^{CC}Ar)$_6$ and W(CN-1-(2-^{i}Pr)-Naph)$_6$ are also lower in more polar solvents (Tables 2 and S3). Compared to toluene solution, ϕ_{PL} drops by 30% for W(CNDipp^{CC}Ph^{OMe})$_6$, 57% for W(CNDipp^{CC}Ph)$_6$ and W(CN-1-(2-^{i}Pr)-Naph)$_6$, 83% for W(CNDipp^{CC}-1-Naph)$_6$, 88% for W(CNDipp^{CC}-9-Phen)$_6$, and >96% for W(CNDipp^{CC}Ph^{CN})$_6$ in THF. For comparison, ϕ_{PL} for W(CNDippPh)$_6$, W(CNDippPh^{OMe2})$_6$, W(CNDippPh^{OMe3})$_6$, and W(CNDippPh^{Ph})$_6$ decrease by 49, 50, 39, and 84%, respectively. These values are in line with the magnitude of charge transfer and associated nonradiative excited-state decay expected for the different complexes.

Excited-State Dynamics and Reduction Potentials. The time-resolved luminescence traces of *W(CNDipp^{CC}Ar)$_6$ and *W(CN-1-(2-^{i}Pr)-Naph)$_6$ in deaerated room temperature toluene solution are shown in Figure 4, and those in 2-MeTHF and THF are shown in Figures S182 and S183, respectively. These measurements show that the excited-state lifetimes of these complexes depend strongly on the solvent polarity, with τ(^{3}MLCT) being hundreds of nanoseconds or several

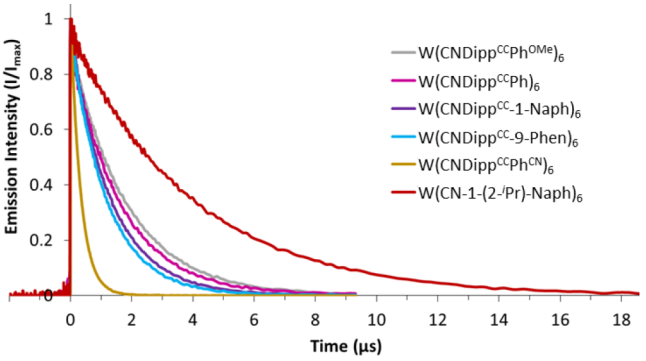

Figure 4. Time-resolved luminescence traces of W(CNDipp^{CC}Ar)$_6$ and W(CN-1-(2-^{i}Pr)-Naph)$_6$ complexes in deaerated room temperature toluene solution.

https://dx.doi.org/10.1021/acs.inorgchem.0c02912
Inorg. Chem. 2021, 60, 3481−3491

microseconds in toluene but decreasing substantially in 2-MeTHF and THF (Tables 2 and S3). This finding is in agreement with the greater distortions observed for *W(CNDipp^{CC}Ar)$_6$ or *W(CN-1-(2-^{i}Pr)-Naph)$_6$ in 2-MeTHF and THF versus toluene solution (vide supra).

Like *W(CNDippAr)$_6$, the excited-state dynamics of *W(CNDipp^{CC}Ar)$_6$ are governed by nonradiative decay. Whereas the radiative decay rate constant (k_r) remains relatively constant for a given complex in all three solvents, the nonradiative decay constant (k_{nr}) is much larger in more polar THF (Table 2). As a result, the lifetimes of *W(CNDipp^{CC}Ar)$_6$ and *W(CN-1-(2-^{i}Pr)-Naph)$_6$ decrease in the order toluene > 2-MeTHF > THF. In alignment with their other photophysical properties, the drop in τ(*W(CNDipp^{CC}Ar)$_6$) is more drastic in the order Ph^{OMe} < Ph < 1-Naph < 9-Phen < Ph^{CN}, with corresponding k_{nr}(THF)/k_{nr}(toluene) ratios of 2.6 < 2.8 < 9.0 < 10.7 < 59, respectively. For W(CN-1-(2-^{i}Pr)-Naph)$_6$, k_{nr}(THF)/k_{nr}(toluene) = 2.1.

That W(CN-1-(2-^{i}Pr)-Naph)$_6$ exhibits the longest τ(^{3}MLCT) among all W(CNAr)$_6$ complexes in all three solvents is noteworthy. In contrast to W(CNDippAr)$_6$ and W(CNDipp^{CC}Ar)$_6$ complexes, which have radially extended and exposed aromatic systems, the expanded π-system in W(CN-1-(2-^{i}Pr)-Naph)$_6$, which remains mostly within the primary coordination sphere, is less accessible. In addition to protecting the tungsten center in the excited state, the sterics resulting from the use of 2-isopropylnaphthyl (rather than 2,6-diisopropylphenyl) isocyanide appear to lock the ligands well in place (Figure 2). This increased rigidity favors longer *W(CN-1-(2-^{i}Pr)-Naph)$_6$ lifetimes. A similar increase in framework rigidity likely accounts for the more favorable photophysical properties, including increased τ(^{3}MLCT) and ϕ_{PL}, observed upon augmentation of the sterics from Mo(CN^{Me}Ar$_3$NC)$_3$ to Mo(CN$^{t\text{Bu}}$Ar$_3$NC)$_3$.[14,40]

In addition to the solvent-polarity dependence of *W(CNDipp^{CC}Ar)$_6$ lifetimes, τ(^{3}MLCT) for these complexes decreases in the order Ph^{OMe} > Ph > 1-Naph > 9-Phen > Ph^{CN} in a given solvent. Notably, variation of k_{nr} with the excited-state energy is consistent with the theory of nonradiative electronic energy relaxation.[41,42] As with electron-transfer reactions in the inverted driving-force regime,[43] the specific rate of a nonradiative transition between two states with nested potential energy surfaces increases as the energy difference between the states decreases. We have modeled the 77 K steady-state luminescence spectra of the W(CNDipp^{CC}Ar)$_6$ complexes (vide infra) and find that they all can be described by effective reorganization energies of 0.19−0.21 eV. These modest distortions, coupled with 1.6−2.0 eV excited-state energies, confirm that the *W(CNDipp^{CC}Ar)$_6$ potential energy surfaces are sequestered well within the boundaries of the ground-state surfaces. Hence, plots of ln(k_{nr}) versus $E_{em,max}$ for W(CNDipp^{CC}Ar)$_6$ are linear (Figure 5), consistent with the predictions of the weak-coupling limit of nonradiative decay theory.[44] $E_{em,max}$ also correlates with the Hammett constants (Figure S168), arguably offering a rational method for designing W(CNDipp^{CC}Ar)$_6$ complexes with desired photophysical properties for targeted applications.

Plots of ln(k_{nr}) versus $E_{em,max}$ for W(CNDippAr)$_6$ complexes display linear fits with R^2 values of 0.81 and 1.00 in toluene and THF, respectively (Figure S169), which is unsurprising given the similar excited-state dynamics of *W(CNDippAr)$_6$ and

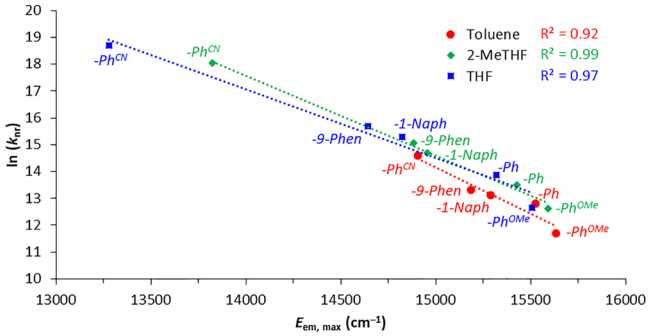

Figure 5. Plots of ln(k_{nr}) versus $E_{em,max}$ for W(CNDipp^{CC}Ar)$_6$ complexes. Best linear fit R^2 values: toluene, 0.92; 2-MeTHF, 0.99; THF, 0.97.

*W(CNDipp^{CC}Ar)$_6$ (vide supra). However, it is worth noting that the latter cover a wider range of ln(k_{nr}) and $E_{em,max}$ values.

*W(CNDipp^{CC}Ar)$_6$ and *W(CN-1-(2-^{i}Pr)-Naph)$_6$ are longer-lived in toluene and 2-MeTHF 77 K glass (Figures S184 and S185 and Table S4). Like W(CNDippAr)$_6$ compounds, the absence of single-exponential decay kinetics in these frozen matrices is attributed to a distribution of ligand conformations. This conformer distribution is expected to be more prominent for W(CNDipp^{CC}Ar)$_6$ complexes, where rotation of the peripheral aromatic system is more facile. Inspection of the 77 K steady-state luminescence spectra also supports this hypothesis. In contrast to the rigidochromism observed for M(CNAr)$_6$ (M = Cr, Mo, W; Ar = Ph, Dipp)[18] and related Re(CNAr)$_5$(CN−B(C$_6$F$_5$)$_3$) (Ar = 2,4,6-C$_6$H$_2$Cl$_3$, 4-C$_6$H$_4$(SF$_5$), 3,5-C$_6$H$_3$(CF$_3$)$_2$, 4-C$_6$H$_4$(COOEt)) MLCT emitters,[45] the emission maxima of W(CNDipp^{CC}Ar)$_6$ complexes in toluene and 2-MeTHF red-shift by 280−540 and 220−360 cm^{-1}, respectively, upon cooling from room temperature to 77 K (Figures S155 and S156).[46] For W(CNDippAr)$_6$ complexes, the emission maxima do not differ significantly between toluene room temperature solution and 77 K glass (Figure S157), whereas we observe a modest blue-shift in $E_{em,max}$ when W(CN-1-(2-^{i}Pr)-Naph)$_6$ is cooled to 77 K in toluene and 2-MeTHF (Figure S149). Thus, we ascribe the movement of $E_{em,max}$ to lower energy to the adoption of more planar, and thus more conjugated and lower energy, CNDipp^{CC}Ar conformers in *W(CNDipp^{CC}Ar)$_6$. Interestingly, the 77 K lifetimes of these excited states follow the same trend observed in room temperature solution, decreasing in the order Ph^{OMe} > Ph > 1-Naph > 9-Phen > Ph^{CN} (Figures S184 and S185 and Table S4).

Franck−Condon modeling of the 77 K W(CNAr)$_6$ steady-state luminescence spectra required three quantum modes and one classical distortion to adequately reproduce the experimental spectra (see the Supporting Information). Fits to the 77 K spectra in toluene were somewhat better than those for 2-MeTHF, so the following discussion focuses on the toluene spectra. The distorting vibrations all are consistent with the ^{3}MLCT character of the luminescent excited state. The highest energy quantum mode (1900−2000 cm^{-1}) is attributable to a distortion in the C$_{isocyanide}$≡N bond. Fits to the W(CNDipp^{CC}Ar)$_6$ spectra require slightly larger distortions in this high-frequency vibration than do the W(CNDippAr)$_6$ spectra, possibly due to an additional small distortion in the C$_{alkynyl}$≡C bond (ca. 2200 cm^{-1}). Overall, the high-frequency mode distortion contributes about 21−22% of the total reorganization in W(CNDipp^{CC}Ar)$_6$ and less than 13% in

https://dx.doi.org/10.1021/acs.inorgchem.0c02912
Inorg. Chem. 2021, 60, 3481−3491

$W(CNDippAr)_6$ and $W(CN\text{-}1\text{-}(2\text{-}^i Pr)\text{-}Naph)_6$. Distortions in the 1200−1400 cm^{-1} modes contribute 15−20% of the total reorganization in all $W(CNAr)_6$ luminescence spectra. These modes likely arise from distortions in the aromatic rings of the arylisocyanide ligands. A low-frequency vibration attributable to W−C stretches (400−500 cm^{-1}) represents 20−30% of the excited-state distortion. The remaining 40−50% of the reorganization energy is modeled with a classical mode representing solvent and low-frequency vibrations of the molecules. This Gaussian envelope also accounts for broadening of the spectra due to inhomogeneities in the solvation environments of the chromophores. The mean reorganization energy for $^*W(CNAr)_6$ in toluene is 0.19 ± 0.03 (2σ) eV.

It is also interesting to note that, despite the lower energy gap between the ground and excited states of $W(CNDipp^{CC}Ar)_6$ (Ar = Ph^{OMe}, Ph, 1-Naph, 9-Phen) relative to $W(CNDippAr)_6$ in toluene solution, both series of complexes exhibit similarly slow nonradiative relaxation and, by extension, comparable ϕ_{PL} and $\tau(^3MLCT)$. Qualitatively, this is consistent with the greater degree of conjugation in the acceptor $CNDipp^{CC}Ar$ ligands, which facilitates greater delocalization of the excited-state electron density, which, in turn, helps to minimize excited-state bond distortions.[22,47] However, the benefits of such delocalization effects are likely counteracted to some extent by the lower rigidity of the secondary aromatic system in $CNDipp^{CC}Ar$ versus CNDippAr ligands.[48]

Encouraged by the promising photophysical properties of $W(CN\text{-}1\text{-}(2\text{-}^i Pr)\text{-}Naph)_6$ and $W(CNDipp^{CC}Ar)_6$ complexes, we next explored their electrochemistry. Like their predecessors, $W(CN\text{-}1\text{-}(2\text{-}^i Pr)\text{-}Naph)_6$ and $W(CNDipp^{CC}Ar)_6$ complexes exhibit electrochemically reversible $W^{[+/0]}$ couples in the narrow range of −0.47 to −0.30 V vs $Fc^{[+/0]}$ (Figure 6 and Table 3). Only irreversible oxidation events are observed at more positive potentials (Figure S204). Alternatively, upon scanning cathodically of the $W^{[+/0]}$ wave of $W(CNDipp^{CC}\text{-}1\text{-}Naph)_6$, $W(CNDipp^{CC}\text{-}9\text{-}Phen)_6$, and $W(CNDipp^{CC}Ph^{CN})_6$, a quasi-reversible reduction event is observed. The current passed during this redox event is much larger than that of the $W^{[+/0]}$ couple. Furthermore, the formal potential of the wave is highly sensitive to the identity of the $CNDipp^{CC}Ar$ secondary aromatic group. Thus, we assign this wave to a ligand-centered reduction rather than a metal-based $W^{[0/-]}$ couple. Consistent with this assignment, $E(CNDipp^{CC}Ar^{[0/-]})$ shifts to more negative potentials and becomes less reversible as the electron-withdrawing nature of the secondary aromatic group decreases according to Ph^{CN} > 9-Phen > 1-Naph > Ph > Ph^{OMe} (Figure S204). Moreover, a linear correlation is observed for plots of E_{00} or $E_{abs,max}$ versus the potential difference between the tungsten-centered oxidation and isocyanide ligand-centered reduction (Figures S205 and S206).

The $W^{[+/0]}$ couples also depend on the nature of the secondary aromatic system in the $CNDipp^{CC}Ar$ framework, albeit to a lesser extent. Notably, the $E(W^{[+/0]})$ values correlate linearly with the Hammett constants[39] (σ; R^2 = 0.99) when $W(CNDipp^{CC}Ph)_6$ is taken as the base complex (σ = 0; Figure 6). Thus, $W(CNDipp^{CC}Ph^{CN})_6$, having the largest σ value and a strongly electron-withdrawing substituent, features the most anodic $W^{[+/0]}$ wave (E = −0.30 V vs $Fc^{[+/0]}$) among this series of compounds. This redox couple shifts cathodically as the electron-withdrawing capability of the peripheral aromatic system decreases in the order 9-Phen (−0.36 V) ≈ 1-Naph (−0.37 V) > Ph (−0.39 V) > Ph^{OMe} (−0.42 V; Table 3). That

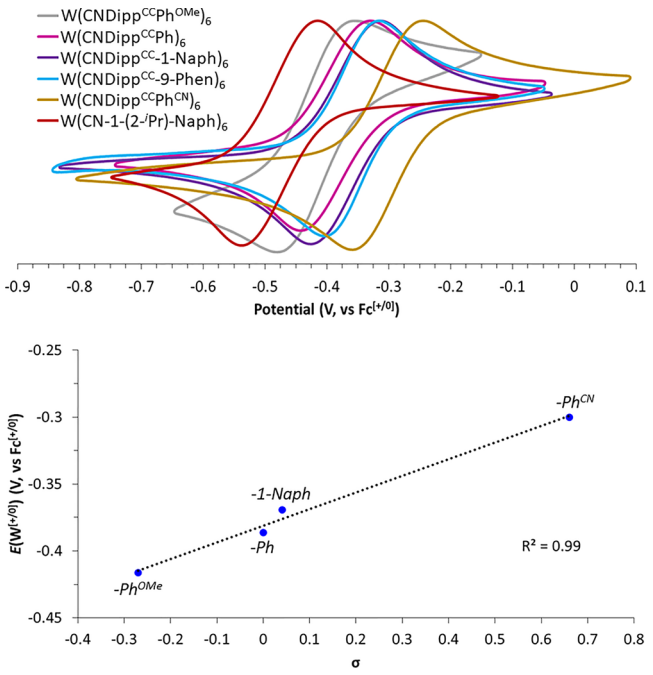

Figure 6. (Top) Cyclic voltammograms of $W(CNDipp^{CC}Ar)_6$ and $W(CN\text{-}1\text{-}(2\text{-}^i Pr)\text{-}Naph)_6$ complexes depicting the isolated $W^{[+/0]}$ redox couple at a scan rate of 100 mV s^{-1} in THF with 0.1 M $[^n Bu_4N][PF_6]$ supporting electrolyte (referenced vs $Fc^{[+/0]}$). (Bottom) Plot of $E(W^{[+/0]})$ versus the Hammett constant for $W(CNDipp^{CC}Ar)_6$ complexes (taking σ(Ph) = 0).

Table 3. Ground- and Excited-State Reduction Potentials of $W(CNAr)_6$ Complexes (V vs $Fc^{[+/0]}$)

$W(CNAr)_6$	$E(W^{[+/0]})$	E_{00}[a]	$E(W^+/^*W^0)$
$W(CNDipp)_6$	−0.72[b]	2.28	−3.00
$W(CNDippPh)_6$	−0.68[b]	2.12	−2.80
$W(CNDippPh^{OMe2})_6$	−0.65[b]	2.14	−2.79
$W(CNDippPh^{OMe3})_6$	−0.65[b]	2.15	−2.80
$W(CNDippPh^{Ph})_6$	−0.67[b]	2.08	−2.75
$W(CNDipp^{CC}Ph^{OMe})_6$	−0.42[c]	2.01	−2.43
$W(CNDipp^{CC}Ph)_6$	−0.39[c]	1.99	−2.38
$W(CNDipp^{CC}\text{-}1\text{-}Naph)_6$	−0.37[c]	1.94	−2.31
$W(CNDipp^{CC}\text{-}9\text{-}Phen)_6$	−0.36[c]	1.93	−2.29
$W(CNDipp^{CC}Ph^{CN})_6$	−0.30[c]	1.89	−2.19
$W(CN\text{-}1\text{-}(2\text{-}^i Pr)\text{-}Naph)_6$	−0.47[c]	2.02	−2.49

[a]In eV. [b]Data from ref 21. Electrochemical measurements performed in CH_2Cl_2 with 0.5 M $[^n Bu_4N][PF_6]$ supporting electrolyte. For $W(CNDipp)_6$, $E(W^{[+/0]})$ and $E(W^+/^*W^0)$ in THF are −0.53 and −2.80 V, respectively.[20] [c]Electrochemical measurements performed in THF with 0.1 M $[^n Bu_4N][PF_6]$ supporting electrolyte.

$E(W^{[+/0]})$ only varies by ca. 120 mV over this set of $W(CNDipp^{CC}Ar)_6$ complexes is consistent with the electronic variations taking place at sites far removed from the tungsten center. For comparison, $E(Mn^{[2+/+]})$ of related 4-substituted phenylisocyanide manganese(I) complexes, $Mn(CNPh^R)_6^+$, span a range of 410 mV when the substituent is varied from R = CN to OMe.[49]

The E_{00} energies of $W(CN\text{-}1\text{-}(2\text{-}^i Pr)\text{-}Naph)_6$ and $W(CNDipp^{CC}Ar)_6$ complexes (estimated from the onset of emission in their 77 K steady-state luminescence spectra in 2-MeTHF) also span a small range (0.13 eV; Table 3). As expected, these energies are smaller than those of W-

https://dx.doi.org/10.1021/acs.inorgchem.0c02912
Inorg. Chem. 2021, 60, 3481−3491

$(CNDippAr)_6$ complexes and, for $W(CNDipp^{CC}Ar)_6$, decrease in the order Ph^{OMe} > Ph > 1-Naph > 9-Phen > Ph^{CN}.

Combining ground-state $W^{[+/0]}$ couples with E_{00} energies yields the excited-state reduction potentials listed in Table 3. In agreement with the photophysical and electrochemical data discussed above, $E(W^+/{*}W^0)$ for $W(CN\text{-}1\text{-}(2\text{-}^i Pr)\text{-}Naph)_6$ and $W(CNDipp^{CC}Ar)_6$ complexes are attenuated with respect to $W(CNDipp)_6$ and $W(CNDippAr)_6$. However, their excited-state reduction potentials are complementary to the latter and can be readily tuned by the judicious choice of a highly modular arylisocyanide ligand. Importantly, $*W(CN\text{-}1\text{-}(2\text{-}^i Pr)\text{-}Naph)_6$ and $*W(CNDipp^{CC}Ar)_6$ are much stronger photoreductants than $*[fac\text{-}Ir(ppy)_3]$ and $*Ru(bpy)_3^{2+}$. That $W(CNDipp^{CC}Ph^{OMe})_6$ and $W(CN\text{-}1\text{-}(2\text{-}^i Pr)\text{-}Naph)_6$ have $E(W^+/{*}W^0) \approx -2.5$ V vs $Fc^{[+/0]}$, long excited-state lifetimes, and, in the case of the former, a high quantum yield (ϕ_{PL} = 0.55) in THF confirms that these complexes are promising photoredox reagents.

CONCLUSIONS

We have synthesized and fully characterized homoleptic tungsten(0) fused-ring and alkynyl-bridged arylisocyanide photoreductants. Notably, the properties of $W(CNDipp^{CC}Ar)_6$ excited states are highly dependent on the identity of the secondary aromatic system, providing a facile route by which they can be tuned. $W(CN\text{-}1\text{-}(2\text{-}^i Pr)\text{-}Naph)_6$ features the longest room temperature solution excited-state lifetime observed to date for $W(CNAr)_6$ complexes, demonstrating the potential benefit of employing fused-ring arylisocyanide ligands in the design of this class of photoreductants. Ongoing work is aimed at assessing the potential of $W(CNDipp^{CC}Ph^{OMe})_6$ and $W(CN\text{-}1\text{-}(2\text{-}^i Pr)\text{-}Naph)_6$ to serve as near-IR two-photon redox catalysts for organic transformations.

ASSOCIATED CONTENT

Supporting Information

The Supporting Information is available free of charge at https://pubs.acs.org/doi/10.1021/acs.inorgchem.0c02912.

Experimental details, synthetic procedures, and compound characterization data, including ^1H and ^{13}C NMR spectra, IR spectra, UV−visible absorbance spectra, steady-state and time-resolved luminescence spectra, cyclic voltammograms, and XRD refinement details (PDF)

Accession Codes

CCDC 2034771−2034777 contain the supplementary crystallographic data for this paper. These data can be obtained free of charge via www.ccdc.cam.ac.uk/data_request/cif, or by emailing data_request@ccdc.cam.ac.uk, or by contacting The Cambridge Crystallographic Data Centre, 12 Union Road, Cambridge CB2 1EZ, UK; fax: +44 1223 336033.

AUTHOR INFORMATION

Corresponding Authors

Jay R. Winkler − *Beckman Institute, California Institute of Technology (Caltech), Pasadena, California 91125, United States;* orcid.org/0000-0002-4453-9716; Email: winklerj@caltech.edu

Harry B. Gray − *Beckman Institute, California Institute of Technology (Caltech), Pasadena, California 91125, United States;* orcid.org/0000-0002-7937-7876; Email: hbgray@caltech.edu

Authors

Javier Fajardo, Jr. − *Beckman Institute, California Institute of Technology (Caltech), Pasadena, California 91125, United States;* orcid.org/0000-0003-0612-7953

Josef Schwan − *Beckman Institute, California Institute of Technology (Caltech), Pasadena, California 91125, United States*

Wesley W. Kramer − *Beckman Institute, California Institute of Technology (Caltech), Pasadena, California 91125, United States*

Michael K. Takase − *Beckman Institute, California Institute of Technology (Caltech), Pasadena, California 91125, United States*

Complete contact information is available at: https://pubs.acs.org/10.1021/acs.inorgchem.0c02912

Author Contributions

All authors have given approval to the final version of the manuscript.

Funding

This work was supported by the National Science Foundation (Grant CHE-1763429) and the Beckman Institute Laser Resource Center, supported by the Arnold and Mabel Beckman Foundation.

Notes

The authors declare no competing financial interest.

ACKNOWLEDGMENTS

We thank Dr. David VanderVelde and Lawrence M. Henling for assistance with NMR and XRD experiments, respectively. The X-ray Crystallography Facility in the Beckman Institute at Caltech was supported by the Dow Next Generation Instrumentation Grant.

REFERENCES

(1) Hagfeldt, A.; Boschloo, G.; Sun, L.; Kloo, L.; Pettersson, H. Dye-Sensitized Solar Cells. *Chem. Rev.* **2010**, *110*, 6595−6663.

(2) Prier, C. K.; Rankic, D. A.; MacMillan, D. W. C. Visible Light Photoredox Catalysis with Transition Metal Complexes: Applications in Organic Synthesis. *Chem. Rev.* **2013**, *113*, 5322−5363.

(3) Glaser, F.; Wenger, O. S. Recent Progress in the Development of Transition-Metal Based Photoredox Catalysts. *Coord. Chem. Rev.* **2020**, *405*, 213129.

(4) Yersin, H.; Rausch, A. F.; Czerwieniec, R.; Hofbeck, T.; Fischer, T. The Triplet State of Organo-Transition Metal Compounds. Triplet Harvesting and Singlet Harvesting for Efficient OLEDs. *Coord. Chem. Rev.* **2011**, *255*, 2622−2652.

(5) Zhao, Q.; Huang, C.; Li, F. Phosphorescent Heavy-Metal Complexes for Bioimaging. *Chem. Soc. Rev.* **2011**, *40*, 2508−2524.

(6) Juris, A.; Balzani, V.; Barigelletti, F.; Campagna, S.; Belser, P.; von Zelewsky, A. Ru(II) Polypyridine Complexes: Photophysics, Photochemistry, Eletrochemistry, and Chemiluminescence. *Coord. Chem. Rev.* **1988**, *84*, 85−277.

(7) Campagna, S.; Puntoriero, F.; Nastasi, F.; Bergamini, G.; Balzani, V. Photochemistry and Photophysics of Coordination Compounds: Ruthenium. *Photochemistry and Photophysics of Coordination Compounds I*; Springer: Berlin, 2007; Vol. *280*, pp 117−214.

(8) Lowry, M. S.; Bernhard, S. Synthetically Tailored Excited States: Phosphorescent, Cyclometalated Iridium(III) Complexes and Their Applications. *Chem. - Eur. J.* **2006**, *12*, 7970−7977.

(9) Flamigni, L.; Barbieri, A.; Sabatini, C.; Ventura, B.; Barigelletti, F. Photochemistry and Photophysics of Coordination Compounds:

Iridium. *Photochemistry and Photophysics of Coordination Compounds II*; Springer: Berlin, 2007; Vol. *281*, pp 143−203.
(10) Arias-Rotondo, D. M.; McCusker, J. K. The Photophysics of Photoredox Catalysis: A Roadmap for Catalyst Design. *Chem. Soc. Rev.* **2016**, *45*, 5803−5820.
(11) Wenger, O. S. Photoactive Complexes with Earth-Abundant Metals. *J. Am. Chem. Soc.* **2018**, *140*, 13522−13533.
(12) Büldt, L. A.; Wenger, O. S. Luminescent Complexes Made from Chelating Isocyanide Ligands and Earth-Abundant Metals. *Dalton Trans.* **2017**, *46*, 15175−15177.
(13) Büldt, L. A.; Wenger, O. S. Chromium(0), Molybdenum(0), and Tungsten(0) Isocyanide Complexes as Luminophores and Photosensitizers with Long-Lived Excited States. *Angew. Chem., Int. Ed.* **2017**, *56*, 5676−5682.
(14) Herr, P.; Glaser, F.; Büldt, L. A.; Larsen, C. B.; Wenger, O. S. Long-Lived, Strongly Emissive, and Highly Reducing Excited States in Mo(0) Complexes with Chelating Isocyanides. *J. Am. Chem. Soc.* **2019**, *141*, 14394−14402.
(15) Büldt, L. A.; Guo, X.; Prescimone, A.; Wenger, O. S. A Molybdenum(0) Isocyanide Analogue of Ru(2,2'-Bipyridine)$_3^{2+}$: A Strong Reductant for Photoredox Catalysis. *Angew. Chem., Int. Ed.* **2016**, *55*, 11247−11250.
(16) Büldt, L. A.; Guo, X.; Vogel, R.; Prescimone, A.; Wenger, O. S. A Tris(Diisocyanide)Chromium(0) Complex Is a Luminescent Analog of Fe(2,2'-Bipyridine)$_3^{2+}$. *J. Am. Chem. Soc.* **2017**, *139*, 985−992.
(17) Mann, K. R.; Cimolino, M.; Geoffroy, G. L.; Hammond, G. S.; Orio, A. A.; Albertin, G.; Gray, H. B. Electronic Structures and Spectra of Hexakisphenylisocyanide Complexes of Cr(0), Mo(0), W(0), Mn(I), and Mn(II). *Inorg. Chim. Acta* **1976**, *16*, 97−101.
(18) Mann, K. R.; Gray, H. B.; Hammond, G. S. Excited-State Reactivity Patterns of Hexakisarylisocyano Complexes of Chromium(0), Molybdenum(0), and Tungsten(0). *J. Am. Chem. Soc.* **1977**, *99*, 306−307.
(19) Gray, H. B.; Mann, K. R.; Lewis, N. S.; Thich, J. A.; Richman, R. M. Photochemistry of Metal-Isocyanide Complexes and Its Possible Relevance to Solar Energy Conversion. *Inorganic and Organometallic Photochemistry*; American Chemical Society, 1978; Vol. *168*, pp 44−56.
(20) Sattler, W.; Ener, M. E.; Blakemore, J. D.; Rachford, A. A.; LaBeaume, P. J.; Thackeray, J. W.; Cameron, J. F.; Winkler, J. R.; Gray, H. B. Generation of Powerful Tungsten Reductants by Visible Light Excitation. *J. Am. Chem. Soc.* **2013**, *135*, 10614−10617.
(21) Sattler, W.; Henling, L. M.; Winkler, J. R.; Gray, H. B. Bespoke Photoreductants: Tungsten Arylisocyanides. *J. Am. Chem. Soc.* **2015**, *137*, 1198−1205.
(22) Kvapilová, H.; Sattler, W.; Sattler, A.; Sazanovich, I. V.; Clark, I. P.; Towrie, M.; Gray, H. B.; Záliš, S.; Vlček, A. Electronic Excited States of Tungsten(0) Arylisocyanides. *Inorg. Chem.* **2015**, *54*, 8518−8528.
(23) Takematsu, K.; Wehlin, S. A. M.; Sattler, W.; Winkler, J. R.; Gray, H. B. Two-Photon Spectroscopy of Tungsten(0) Arylisocyanides Using Nanosecond-Pulsed Excitation. *Dalton Trans.* **2017**, *46*, 13188−13193.
(24) Chen, Y.; Guan, R.; Zhang, C.; Huang, J.; Ji, L.; Chao, H. Two-Photon Luminescent Metal Complexes for Bioimaging and Cancer Phototherapy. *Coord. Chem. Rev.* **2016**, *310*, 16−40.
(25) Li, H.; Yang, Y.; He, C.; Zeng, L.; Duan, C. Mixed-Ligand Metal−Organic Framework for Two-Photon Responsive Photocatalytic C−N and C−C Coupling Reactions. *ACS Catal.* **2019**, *9*, 422−430.
(26) Markham, J. J. Interaction of Normal Modes with Electron Traps. *Rev. Mod. Phys.* **1959**, *31*, 956−989.
(27) Ansbacher, F. A Note on the Overlap Integral of Two Harmonic Oscillator Wave Functions. *Z. Naturforsch., A: Phys. Sci.* **1959**, *14a*, 889−892.
(28) Sheldrick, G. M. Phase Annealing in SHELX-90: Direct Methods for Larger Structures. *Acta Crystallogr., Sect. A: Found. Crystallogr.* **1990**, *A46*, 467−473.
(29) Sheldrick, G. M. Crystal Structure Refinement with SHELXL. *Acta Crystallogr., Sect. C: Struct. Chem.* **2015**, *C71*, 3−8.
(30) Müller, P. Practical Suggestions for Better Crystal Structures. *Crystallogr. Rev.* **2009**, *15*, 57−83.
(31) Favale, J. M.; Danilov, E. O.; Yarnell, J. E.; Castellano, F. N. Photophysical Processes in Rhenium(I) Diiminetricarbonyl Arylisocyanides Featuring Three Interacting Triplet Excited States. *Inorg. Chem.* **2019**, *58*, 8750−8762.
(32) Dong, Y.; Jv, J.-J.; Wu, X.-W.; Kan, J.-L.; Lin, T.; Dong, Y.-B. A Palladium−Carbon-Connected Organometallic Framework and Its Catalytic Application. *Chem. Commun.* **2019**, *55*, 14414−14417.
(33) Belcher, R.; Lyle, S. J.; Stephen, W. I. The Preparation of Some New Substituted Naphthylamines and Naphthidines. *J. Chem. Soc.* **1958**, 3243−3248.
(34) Davalli, S.; Lunazzi, L.; Macciantelli, D. Conformational Studies by Dynamic NMR. 40. Conformational Atropoisomerism in Highly Hindered Naphthylamines. *J. Org. Chem.* **1991**, *56*, 1739−1747.
(35) Carnahan, E. M.; Protasiewicz, J. D.; Lippard, S. J. The 15 Years of Reductive Coupling: What Have We Learned? *Acc. Chem. Res.* **1993**, *26*, 90−97.
(36) Lockwood, M. A.; Fanwick, P. E.; Rothwell, I. P. Reactivity of a Tungsten(II) Aryloxide with Isocyanides and Isocyanates. *Organometallics* **1997**, *16*, 3574−3575.
(37) While these angles are calculated using the major component of the disordered structure, the dihedral angles for the minor component do not differ appreciably.
(38) Toyota, S. Rotational Isomerism Involving Acetylene Carbon. *Chem. Rev.* **2010**, *110*, 5398−5424.
(39) Hansch, C.; Leo, A.; Taft, R. W. A Survey of Hammett Substituent Constants and Resonance and Field Parameters. *Chem. Rev.* **1991**, *91*, 165−195.
(40) Herr, P.; Wenger, O. S. Excited-State Relaxation in Luminescent Molybdenum(0) Complexes with Isocyanide Chelate Ligands. *Inorganics* **2020**, *8*, 14.
(41) Robinson, G. W.; Frosch, R. P. Theory of Electronic Energy Relaxation in the Solid Phase. *J. Chem. Phys.* **1962**, *37*, 1962−1973.
(42) Caspar, J. V.; Kober, E. M.; Sullivan, B. P.; Meyer, T. J. Application of the Energy Gap Law to the Decay of Charge-Transfer Excited States. *J. Am. Chem. Soc.* **1982**, *104*, 630−632.
(43) Marcus, R. A.; Sutin, N. Electron Transfers in Chemistry and Biology. *Biochim. Biophys. Acta, Rev. Bioenerg.* **1985**, *811*, 265−322.
(44) Englman, R.; Jortner, J. The Energy Gap Law for Non-Radiative Decay in Large Molecules. *J. Lumin.* **1970**, *1−2*, 134−142.
(45) Chan, K.-C.; Tong, K.-M.; Cheng, S.-C.; Ng, C.-O.; Yiu, S.-M.; Ko, C.-C. Design of Luminescent Isocyano Rhenium(I) Complexes: Photophysics and Effects of the Ancillary Ligands. *Inorg. Chem.* **2018**, *57*, 13963−13972.
(46) Samples of W(CNDipp^{CC}Ph^{CN})$_6$ in 2-MeTHF do not follow this trend, with $E_{em,max}$ instead blue-shifting at 77 K. This is likely the result of significant distortions and solvent interactions of *W(CNDipp^{CC}Ph^{CN})$_6$ in more polar 2-MeTHF at room temperature.
(47) Strouse, G. F.; Schoonover, J. R.; Duesing, R.; Boyde, S.; Jones, W. E., Jr.; Meyer, T. J. Influence of Electronic Delocalization in Metal-to-Ligand Charge Transfer Excited States. *Inorg. Chem.* **1995**, *34*, 473−487.
(48) Treadway, J. A.; Loeb, B.; Lopez, R.; Anderson, P. A.; Keene, F. R.; Meyer, T. J. Effect of Delocalization and Rigidity in the Acceptor Ligand on MLCT Excited-State Decay. *Inorg. Chem.* **1996**, *35*, 2242−2246.
(49) Treichel, P. M.; Mueh, H. J. Electrochemical Studies on [Mn(CNR)$_6$]$^+$ Complexes. *Inorg. Chem.* **1977**, *16*, 1167−1169.

https://dx.doi.org/10.1021/acs.inorgchem.0c02912
Inorg. Chem. 2021, 60, 3481−3491